Automating Heisenberg Hamiltonian Exchange Tensor Derivation via Group Theory

Theodore Beevers[1]

[1]*School of Physics and Astronomy, University of Leeds, Leeds LS2 9JT, United Kingdom*

(Dated: May 14, 2025)

EXECUTIVE SUMMARY

In a magnet, atoms contain electrons that have a property called spin, which has a direction, and can be thought of as a tiny bar magnet. The collective orientation of these spins or bar magnets determines the material's overall magnetisation. Each spin interacts with its neighbours via the exchange interaction, which balances the various energy costs associated with how one spin aligns relative to its neighbour to find the lowest-energy configuration. On any given bond, this interaction is described by nine possible components that together dictate whether the two spins prefer to align parallel, at a fixed angle, or undergo continuous, wave-like motion. Finding the possible interactions between these spins is of great interest because it can lead to magnetic phenomena with exciting future applications. For example, an antisymmetric exchange component can cause spins to collectively twist creating a wave that flows through the system. These currents are known as magnon currents, and are analogous to electric currents, but resistive to thermal energy losses. Knowing which particular exchange interactions are allowed on a bond can uncover such phenomena and allow advances in this area.

Atoms collectively form a crystal, which have symmetry element such as a rotation or inversion, meaning that when applied the symmetry element leaves the crystal looking the same as before. There is a condition called Neumann's principle, which requires the physical properties of a crystal to adhere to the same symmetry requirements. Put simply, this states that if a crystal doesn't change, the laws of physics shouldn't either, and in turn this restricts the physical properties' possible components. An example is when a crystal can be inverted, there can be no total antisymmetric exchange. This principle can be applied at the bond level, and as a result the exchange interaction is restricted by the bonds symmetries. However, an often overlooked fact is that bonds are not necessarily restricted by the same symmetries of the overall crystal, and antisymmetric couplings can still be permitted on bonds in a crystal with an inversion symmetry.

In this project this concept of symmetry was utilised to calculate all allowed interactions between two spins at the bond level. A computer algorithm was developed to automatically determine the symmetry elements of a bond, and these were applied to the bond's exchange interaction components, thus specifying it for the bond. This process avoids the risk of human error, and speeds up otherwise tedious calculations, providing a quick and robust method for checking if a bond can hold certain interactions.

If two bonds can be mapped to one another by a symmetry operation, such as a rotation, then the bonds are equivalent and must hold the same exchange interaction components. However, this is often incorrectly assumed to be the case, and the algorithm developed also has a method of verifying this, which can be used to uncover incorrect predictions.

Models that predict magnon spectra often miss or simplify the full set of bond symmetries, which leads to incorrect results. This is a reason why listing every exchange interaction allowed by a bond's symmetry is important. By using symmetry correctly to identify all possible interactions, models can be built that more accurately describe magnons, helping developments in thermal resistive technologies.

The algorithm has been tested on structures with low symmetry and complex symmetry elements in order to verify its calculations. Bonds in magnetic compounds MnF_2 and $Y_3Fe_5O_{12}$ were put through the algorithm, uncovering symmetrically distinct bonds that were previously assumed to be equivalent, and finding their allowed components, allowing for new interpretations of their properties. The interactions for each bond in Mn_5Ge_3 were found, proving that antisymmetric exchange is allowed in the crystal despite its inversion symmetry. Overall, the algorithm has proved useful in determining allowed interactions in physical systems and should be put to use in many magnetic materials to confirm or correct reported phenomena. The algorithm should also be deployed on magnetic materials with unknown exchange interactions to systematically identify their allowed couplings and guide model construction.

I. INTRODUCTION

A. Exchange

The Pauli exclusion principle forbids two electrons from occupying the same quantum state, and therefore requires the total two-electron wave-function to be antisymmetric. Consequently, either the spatial part of the wave-function is symmetric, forcing the spin part to be antisymmetric, or vice versa [1]. When the spatial wave-function is symmetric, both electrons share the same bonding orbital and their overlap is maximized, which raises the Coulomb repulsion. However, an antisymmetric spatial wave-function pushes electrons into separate regions, creating electron holes around like-spin partners; this reduces Coulomb repulsion but also decreases uncertainty in position, and by the Heisenberg uncertainty principle the corresponding kinetic energy increases. Exchange is a result of the competition between the Coulomb repulsion and kinetic energies [1]. In magnetic materials, atoms host one or more unpaired electrons whose spins are localised at their sites, and the combined magnetic moment of these electrons defines each atom's localised spin. Exchange interactions among these localised atomic spins give rise to spontaneous magnetisation even in the absence of an applied magnetic field [2]. The interactions are characterised by the Hamiltonian for the Heisenberg model [1]

$$H = -\sum_{\langle i,j \rangle} \mathbf{S}_i \cdot \mathbf{J}_{ij} \cdot \mathbf{S}_j, \tag{1}$$

where $\mathbf{S}_i$ and $\mathbf{S}_j$ represent the dimensionless spin vectors at sites i and j, $\sum_{\langle i,j \rangle}$ indicates a summation over all pairs of neighbouring spins, and $\mathbf{J}_{ij}$ is the exchange interaction tensor between spins i and j (in joules)[1]. The negative sign is chosen to result in a decrease in energy when the term $\mathbf{S}_i \cdot \mathbf{J}_{ij} \cdot \mathbf{S}_j$ is positive. In ferromagnets, below the Curie temperature T_c, these exchange forces overcome thermal disorder to sustain a non-zero net magnetisation, but above T_c, thermal fluctuations destroy the long-range spin order and the spontaneous magnetisation vanishes [1, 2].

The tensor can be decomposed into constituent parts describing isotropic, anisotropic and antisymmetric interactions. Often, the anisotropic and antisymmetric contributions are assumed to be zero, and J_{ij} is given by an isotropic scalar quantity. The sign of J_{ij} characterizes whether a material is ferromagnetic (J>0) or antiferromagnetic (J<0), favouring parallel or antiparallel spins respectively [1]. However, anisotropic or antisymmetric exchange is often present, and recent developments have found more materials exhibiting non-zero antisymmetric exchange terms, such as Mn_5Ge_3 [3], CrI_3 [4]. Anisotropic exchange arises whenever the exchange parameter itself becomes bond-dependent so that the coupling strength varies with the orientation of each spin pair relative to the crystallographic bond direction [5]. When these anisotropies are summed over all bonds in the crystal, magnetocrystalline anisotropy arises, making some axes "easy" to magnetise and others "hard." Antisymmetric exchange is known as the Dzyaloshinskii-Moriya interaction (DMI) [6, 7], and it arises as a consequence of spin-orbit coupling (SOC) in one of the magnetic ions. SOC is a relativistic effect where the orbiting electron experiences an orbiting nucleus and a magnetic field induced from this, coupling with its own spin. This creates an excited state, and in turn gives an exchange interaction between the excited state and the ground state of another ion (DMI) [2]. The DM part of the Hamiltonian is given by;

$$H_{DM} = \sum_{\langle i,j \rangle} \mathbf{D}_{ij} \cdot (\mathbf{S}_i \times \mathbf{S}_j), \tag{2}$$

where $\mathbf{D}_{ij} = -\mathbf{D}_{ji}$ is the axial vector (in joules) between the spin sites i and j, mediated by a third site (ligand) in the system [1, 2, 8, 9]. If $\mathbf{D}_{ij}$ is negative, the energy is lowest when $\mathbf{D}_{ij} \parallel (\mathbf{S}_i \times \mathbf{S}_j)$, trying to force the two spins to be at right angles to each other in a plane perpendicular to $\mathbf{D}_{ij}$, consequently canting the spins by a small angle. The canting leads to chiral arrangements and gives rise to spin waves or complex magnetic textures such as spin spirals and skyrmions, which have a wide range of applications [8–12]. The total Hamiltonian can then be broken down as;

$$\begin{aligned} H = &-\sum_{\langle i,j \rangle} J_{ij}^{iso}\, \mathbf{S}_i \cdot \mathbf{S}_j \; - \sum_{\langle i,j \rangle} \mathbf{S}_i \cdot \mathbf{\Gamma}_{ij} \cdot \mathbf{S}_j \\ &+ \sum_{\langle i,j \rangle} \mathbf{D}_{ij} \cdot (\mathbf{S}_i \times \mathbf{S}_j)\,, \end{aligned} \tag{3}$$

where J_{ij}^{iso} represents the symmetric isotropic part of the exchange, $\mathbf{\Gamma}_{ij}$ the symmetric anisotropic exchange, and $\mathbf{D}_{ij}$ the antisymmetric exchange. The full exchange tensor can expressed as a matrix showing the different possible couplings;

$$\mathbf{J}_{ij} = \begin{pmatrix} J_{ij}^{xx} & J_{ij}^{xy} & J_{ij}^{xz} \\ J_{ij}^{yx} & J_{ij}^{yy} & J_{ij}^{yz} \\ J_{ij}^{zx} & J_{ij}^{zy} & J_{ij}^{zz} \end{pmatrix}, \tag{4}$$

or broken down further using Eq. (3), as

$$\begin{aligned} \mathbf{J}_{ij} = J_{ij}^{\mathrm{iso}} \begin{pmatrix} 1 & 0 & 0 \\ 0 & 1 & 0 \\ 0 & 0 & 1 \end{pmatrix} + \begin{pmatrix} \Gamma_{ij}^{xx} & \Gamma_{ij}^{xy} & \Gamma_{ij}^{xz} \\ \Gamma_{ij}^{xy} & \Gamma_{ij}^{yy} & \Gamma_{ij}^{yz} \\ \Gamma_{ij}^{xz} & \Gamma_{ij}^{yz} & \Gamma_{ij}^{zz} \end{pmatrix} \\ + \begin{pmatrix} 0 & D_{ij}^{z} & -D_{ij}^{y} \\ -D_{ij}^{z} & 0 & D_{ij}^{x} \\ D_{ij}^{y} & -D_{ij}^{x} & 0 \end{pmatrix}. \end{aligned} \tag{5}$$

In this project, an automated algorithm has been developed with code to determine, for any bond in a crystal, which components of $\mathbf{J}_{ij}$ are allowed, equivalent or forbidden. Knowing the possible components of $\mathbf{J}_{ij}$ for a bond is vital for understanding and modelling magnetic phenomena. Estab-

lishing whether a bond exhibits anisotropic or antisymmetric couplings can help predict how the spins align, what types of magnetic order and excitations will arise, and help interpret experimental results [1, 3, 5, 13].

It is possible to calculate these constraints manually, however, doing so can be tedious and is prone to errors. Moving to an automatic process means that further research can be done with confidence that there are no omissions of couplings that could be taking place. For a rigorous method, the algorithm was built on the solid basis of group theory, which we will proceed to discuss in detail.

B. Symmetry

All crystals possess some component of symmetry, that is we can apply a symmetry operation S that acts on the positions of atoms in the crystal (C) and transforms them into equivalent positions, and the crystal is left looking the same as before the operation was applied [14],

$$\mathrm{C} = S\mathrm{C}. \tag{6}$$

The mathematics of group theory involves the study of these symmetry operations, and they provide an extremely useful and powerful tool for the completion of the project.

A group is defined by operations that when multiplied give another operation in the group [14]. Each S incorporates a symmetry element R, which is a geometric feature such as an axis of rotation, a reflection or a centre of inversion, and can be expressed as a matrix. They can also contain a translation vector $\mathbf{T}$, so the full symmetry operation $S = (\mathrm{R}, \mathbf{T})$. A symmetry operation S acts on a point x by

$$Sx = \mathrm{R}x + \mathbf{T}. \tag{7}$$

Symmetry operations are carried out with respect to these elements or a combination of them [15]. A space group $\mathbf{G}$ is the full set of symmetry elements combined with the lattice's translational symmetries that when applied leave an entire crystal lattice unchanged, $S \in \mathbf{G}$. Under any space-group symmetry of the crystal, the crystal is carried into itself, leaving the crystal invariant [14]. There are two possible categories for a space group: symmorphic, meaning $\mathbf{G}$ has only a list of operations with no intrinsic translations $S = (\mathrm{R}, \mathbf{0})$, or nonsymmorphic, meaning some symmetry operations of the space group contain an element R and an intrinsic translation $\mathbf{T}$. These compound operations manifest as screw-axis or glide planes [14]. A point group $\mathbf{P}_x$ is the subset of operations that leave at least one point in the crystal fixed. The crystallographic point group $P = \{(R \mid \mathbf{0}) \,\big|\, (R \mid \mathbf{T}) \in G\}$ consists of all symmetry operations in the space group $\mathbf{G}$ once all translations $\mathbf{T}$ have been set to 0 [15]. For crystals there are exactly 230 distinct space groups, and each can be further classified into one of 32 crystallographic point groups [14, 15].

To utilise this concept of symmetry, we can employ Neumann's principle, which states that if a crystal is invariant with respect to a list of symmetry operations, any of its physical properties must also be invariant with respect to the same symmetry operations, or otherwise stated, the symmetry operations of any physical property of a crystal must include the symmetry operations of the point group of the crystal [15, 16]. This imposes constraints on its physical properties, effectively reducing the number of independent components in the tensors that describe these properties. This accounts for physical properties concerning the complete lattice and therefore the material, but can also be applied at the level of bonds. If a symmetry operation leaves a bond invariant, any physical property along that bond also has to respect those symmetry operations. For example, a possible symmetry operation is $S = (C_{2x}, \mathbf{0})$, where C_{2x} denotes a two-fold rotation around the x-axis represented by the matrix

$$C_{2x} = \begin{pmatrix} 1 & 0 & 0 \\ 0 & -1 & 0 \\ 0 & 0 & -1 \end{pmatrix}. \tag{8}$$

This operation will perform the following transformations of coordinates:

$$x \to x,\ y \to -y,\ z \to -z. \tag{9}$$

If a bond $\mathbf{B}_{ij}$ between sites i and j is aligned parallel and along the x-axis, it will be left invariant by this operation. Its corresponding exchange tensor $\mathbf{J}_{ij}$ must also be invariant with respect to these transformations of coordinates, and we can use Fumi's method [16] to quickly see how the components will transform under this operation. We convert all axis labels as in Eq. (9), and under the operation, the components of $\mathbf{J}_{ij}$ transform as;

$$\begin{aligned} J_{ij}^{xy} &\to -J_{ij}^{xy}, J_{ij}^{xz} \to -J_{ij}^{xz}, \\ J_{ij}^{yx} &\to -J_{ij}^{yx}, J_{ij}^{zx} \to -J_{ij}^{zx}, \end{aligned} \tag{10}$$

and all other components are left unchanged. The invariance condition then gives the following equivalencies:

$$\begin{aligned} J_{ij}^{xy} &= -J_{ij}^{xy}, J_{ij}^{xz} = -J_{ij}^{xz}, \\ J_{ij}^{yx} &= -J_{ij}^{yx}, J_{ij}^{zx} = -J_{ij}^{zx}, \end{aligned} \tag{11}$$

resulting in the solutions:

$$J_{ij}^{xy} = 0, J_{ij}^{xz} = 0, J_{ij}^{yx} = 0, J_{ij}^{zx} = 0. \tag{12}$$

Thus these components are 'forbidden', and all other components are 'allowed' under this operation. A symmetry operation can also cause different components to be equal, giving 'equivalencies' in the full tensor of $\mathbf{J}_{ij}$ (Eq. 4).

A bond is left invariant by a symmetry operation if the resulting bond differs only by a pure lattice translation or is placed in a position of an equivalent bond within the unit cell.

The stabilizer group $\mathbf{G}_{ij}$ of a bond between sites i and j is the set of all operations that leave the bond invariant [17] and is given by;

$$\begin{aligned}\mathbf{G}_{ij} = \{S \in \mathbf{G} : \{\mathrm{R}\mathbf{A}_i + \mathbf{T},\ \mathrm{R}\mathbf{A}_j + \mathbf{T}\} \\ = \{\mathbf{A}_i, \mathbf{A}_j\} \bmod \mathrm{L}\},\end{aligned} \tag{13}$$

where $\{\mathbf{A}_i, \mathbf{A}_j\}$ is the unordered pair of position vectors of the endpoints of the bond invariant modulo the Bravais lattice L, and S denotes a space-group operation with symmetry element R and translation vector $\mathbf{T}$. $\mathbf{G}_{ij}$ is is contained within the entire space group of that crystal $\mathbf{G}_{ij} \subset \mathbf{G}$. In order to obtain the point group of the bond $\mathbf{P}_{ij}$, we take all $S \in \mathbf{G}_{ij}$ and set all translations to $\mathbf{0}$, $\mathbf{P}_{ij} = \{S \in \mathbf{G}_{ij}, S = (\mathrm{R}, \mathbf{T} = \mathbf{0})\}$. It is now possible to apply these point group operations to the exchange tensor describing this bond to specify and reduce the number of allowed components, and identify which components remain invariant under these operations, in accordance with Neumann's principle. Mathematically, this is expressed in index form as;

$$\mathrm{T}_{ijk\ldots n} = a_{ip}\, a_{jq}\, a_{kr} \ldots a_{nu}\, \mathrm{T}_{pqr\ldots u}, \tag{14}$$

where $\mathrm{T}_{pqr\ldots u}$ is the tensor in the original coordinate system, $\mathrm{T}_{ijk\ldots n}$ is the transformed tensor, and each a_{ip}.. represents the elements of the symmetry operation matrices that transform the coordinates [16]. The indices represent a left (row) and right (column) multiplication by each symmetry matrix element. For a rank-2 tensor T, this is expressed in matrix notation as

$$\mathrm{T} = A\mathrm{T}A^T, \tag{15}$$

where $A = (a_{ip})$ is a 3x3 symmetry matrix. By systematically applying this relation for all symmetry operations of the bond's point group, we can determine the non-zero and independent components of the tensor $\mathbf{J}_{ij}$.

If a bond in the crystal can be mapped onto another using a space group operation S, that is if

$$\mathbf{B}_{kl} = S\mathbf{B}_{ij}, \tag{16}$$

(where $\mathbf{B}_{ij}, \mathbf{B}_{kl}$ represent bonds between atoms $i-j$ and $k-l$), then $\mathbf{B}_{ij}$ and $\mathbf{B}_{kl}$ are said to be in the same orbit X_{ij} [17]. The orbit X_{ij} of a bond under $\mathbf{G}$ is the set of all bonds obtained by applying all $S \in \mathbf{G}$ to the unordered pair of endpoints of the bond $S \cdot \{\mathbf{A}_i, \mathbf{A}_j\}$[17]. All bonds in the same orbit share identical symmetry constraints and hence the same form of exchange tensor. $\mathbf{J}_{ij}$ can be mapped with S to give $\mathbf{J}_{kl}$ using

$$\mathbf{J}_{kl} = \mathrm{R} \cdot \mathbf{J}_{ij} \cdot \mathrm{R}^T, \tag{17}$$

where R represents the symmetry element matrix in S. This expresses the components of the tensor in the rotated frame, so it is possible to see the different isotropic, anisotropic and antisymmetric contributions attributed to this bond.

The code developed implements these group-theoretical methods to determine with clarity which components of a bond's exchange tensor are allowed, and if two bonds can be mapped onto one another so that their tensor entries are equivalent. Automating this procedure eliminates both what would be extensive time spent doing tedious symmetry calculations by hand, and the risk of errors that could come from any part of these calculations.

For the Dzyaloshinskii-Moriya interaction, Moriya established specific rules based on symmetry considerations that determine the existence or direction of the vector $\mathbf{D}_{ij}$ [7]. The most significant of these rules states that if the bond connecting two magnetic ions has an inversion centre (i.e., the bond is centrosymmetric), then the total antisymmetric exchange $\mathbf{D}_{ij}$ of the bond vanishes [7]. This could take affect in the whole crystal, and if the crystal has an inversion centre, the net DMI of the crystal must be zero [7]. Centrosymmetric crystals are usually assumed to exhibit no DMI, however recently discoveries have revealed that even in this case there can still be DMI on the level on individual bonds that lack inversion symmetry, leading to phenomena such as topological magnons and magnetic skrymions [3, 11, 18]. This highlights the importance of considering the symmetries of individual bonds, not just the overall crystal symmetry, when studying magnetic interactions.

C. Motivations

In an ordered ground state of a magnet, all spins are aligned to minimise the overall energy, as evident in Eq. 1. Every spin $\mathbf{S}_i$ sits in an effective exchange field created by its neighbours, so any small tilt away from the ground-state orientation costs exchange energy. There is a restoring torque that makes the spin precess, in turn disturbing its neighbours and causing a spin wave to propagate through the lattice. How exactly a tilt on site i affects a tilt on site j is governed by the exchange tensor $\mathbf{J}_{ij}$. Isotropic, anisotropic and antisymmetric (DM) contributions of $\mathbf{J}_{ij}$ in Eq. (5) can dictate whether spins prefer to stay collinear, cant at a fixed angle, or develop chiral textures. Finding possible non-zero components is essential for predicting the correct spin-wave dynamics in different magnets.

Magnons are the bosonic quasiparticles that arise from the quantisation of these spin waves. They are central to understanding magnetic structures and couplings, and underpin many magnetic phenomena, such as thermal magnetisation decay and phase transitions [19, 20]. Magnon spintronics is the study of spin currents carried by magnons. These currents are analogous to electric currents and can be used to carry, transport and process information, but without inherent disadvantages such as dissipation of energy due to resistive losses [10]. Dzyaloshinskii–Moriya and other antisymmetric or anisotropic exchanges can produce magnons that are topologically stable [3], meaning they cannot be deformed without a significant use of energy, making them resistive to external perturbations such as thermal fluctuations, which could

have implications for dissipationless spin-wave channels aiding spintronics [21, 22]. Magnons provide an incentive to find DMI or anisotropic exchange interactions between bonds, and studying exchange interactions in many materials will allow for further research and developments in this field.

Magnons can be modelled using Linear Spin Wave Theory (LSWT) [13, 23]. LSWT can be derived with the quantum Heisenberg Hamiltonian, and uses Holstein-Primakoff mapping [23] to express spin operators as bosonic operators, truncating the expressions to first order. The Hamiltonian is then expanded to a quadratic term in these operators, giving non-interacting hopping terms, but neglecting higher order interacting parts. The resulting Hamiltonian can be diagonalised to give the magnon dispersion relation, used to calculate the ground state energy and find the temperature dependence of magnetisation [23–25].

LSWT is useful for understanding magnons, but it can overlook symmetries that effect degeneracy in an excited state. The underlying crystal symmetries dictate the form of each $\mathbf{J}_{ij}$, and by Eq. (1), the resulting Hamiltonian H is invariant under those operations. As H is approximated out to the Nth neighbour shell, it only respects the stabilizer symmetries of the included bonds. These bonds could all be in the same orbit X and share one $\mathbf{J}_{ij}$. However, bonds beyond the Nth shell that aren't included in the Hamiltonian can have a non-zero contribution to the exchange energy, and even if these bonds share a shell, they could have different stabilizer groups and not be related by symmetry due to the surrounding environment of non-magnetic ions. These bonds symmetries aren't included giving the Hamiltonian an accidental heightened symmetry. This phenomenon is called a 'shell anomaly' [26]. The spurious symmetry gives extra degeneracies in LSWT that vanish once longer range couplings are included. Improper symmetries can lead to incorrect topological classifications [27, 28], and implementing the correct symmetries is of high importance as it can limit the possible topological band structures that can arise [26], affecting possible dissipationless spintronic devices [10, 21, 22]. Shell anomalies not only take affect in LSWT, but could appear in many tight-binding models, meaning there is an importance in any model to work with the correct symmetries of the lattice and the bonds.

An instructive example of a shell anomaly appears in the collinear antiferromagnet MnF_2, which crystallises in the non-symmorphic rutile structure (space group $P4_2/mnm$). The Mn^{2+} ions form a body-centred tetragonal lattice each surrounded by F^- ions (Fig. 1). Because neighbouring Mn^{2+} sites carry opposite (up and down) spins, it is natural to split the lattice into two sublattices, a and b, each consisting of one Mn^{2+} at its centre plus a surrounding F^- octahedron (Fig. 1b) [1].

In MnF_2, every first-shell exchange bond connects an a site to a b site. These are the bonds connecting the central Mn^{2+} ion to each Mn^{2+} in the 8 corners, and they share one exchange parameter $\mathbf{J}_{bd}$, as each bond can be related using equation (17), sharing an orbital X. This validates the use of a singular parameter for these bonds. Further neighbour couplings $\mathbf{J}_d$ and $\mathbf{J}'_d$ are inequivalent due to the surrounding environments of F^- ions, and therefore a shell anomaly could arise if the couplings are not included in LSWT.

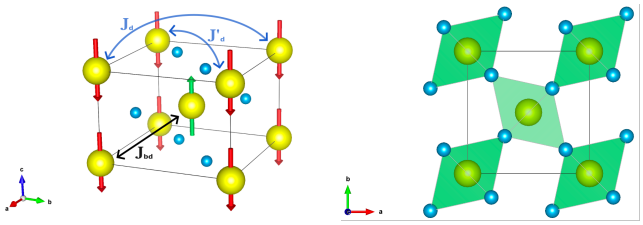

FIG. 1: Crystal structure of the unit cell of MnF_2. (a) Mn^{2+} ions form a body-centred cubic structure, with six F^- ions surrounding the central Mn^{2+} ion. Original figure, but based on figure in [26]. (b) Two sublattices of MnF_2 connected at a corner of each octahedral of fluoride ions centred with an Mn^{2+} ion. The two sublattices have opposite orientations of octahedra and opposite spin. Figures generated with VESTA [29].

If a one-parameter model is used by assigning the same coupling $\mathbf{J}_{bd}$ to all nearest-neighbour $a-b$ bonds, the resulting Hamiltonian becomes invariant under the operation that swaps every a site spin with a b site partner. The $a-b$ interchange is not a symmetry of the true Hamiltonian once further-neighbour couplings ($a-a$ and $b-b$) are included, breaking the symmetry. It's appearance is a result of truncating the exchange to the nearest-neighbour shell, and this accidental enlargement of symmetry is the shell anomaly. LSWT of this model exhibits a two-fold magnon degeneracy everywhere in the Brillouin zone. This is unphysical and vanishes when including the coupling of further neighbours $\mathbf{J}_d$ and $\mathbf{J}'_d$, seen in Fig. (2)[26].

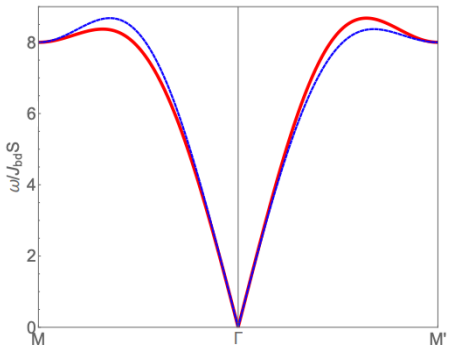

FIG. 2: Magnon spectrum in MnF_2 showing the degeneracy breaking from including the symmetrically inequivalent 3rd NN-shell. Modelled with LSWT using three different exchange parameters, and $\mathbf{J}_d \neq \mathbf{J}'_d$. Figure taken from [26].

It is possible for further neighbour exchange values to be

negligible enough so that the degeneracies are still present up to instrumental resolution, and degeneracy breaking cannot be seen by experiment [26, 30]. This adds vital importance to determining if bonds are symmetrically equivalent, as we cannot rely on data to uncover the unphysical phenomena.

Another consequence of a shell anomaly is that, if the sublattice exchanges $a-a$ and $b-b$ are unequal, fluctuations could tend to reduce the magnetic moments associated with sublattice unequally, allowing a net magnetisation of a material. In this instance an antiferromagnet would become a ferrimagnet [26, 31, 32]. This is an obvious major consequence uncovered by including correct symmetries from longer-range couplings.

As the Hamiltonian is LSWT is expanded to quadratic order, it only includes transverse spin fluctuations $J^{\pm\pm}$, and leaves out transverse-longitudinal components $J^{z\pm}$, as they only enter the theory at cubic or quartic order [33]. LSWT is completely blind to these terms, and this phenomenon is termed "anisotropy blindness" [26]. The exchange tensor without these terms then becomes

$$\mathbf{J}_{ij} = \begin{pmatrix} J_{ij}^{xx} & J_{ij}^{xy} & 0 \\ J_{ij}^{yx} & J_{ij}^{yy} & 0 \\ 0 & 0 & J_{ij}^{zz} \end{pmatrix}, \tag{18}$$

corresponding to an extra two-fold (180°) rotation C_2 of the spins around the z-axis. However, it is of course possible for bonds to have these missing symmetric anisotropic or antisymmetric terms, when there is spin-orbit coupling involved with the bond. Without these components, LSWT could can predict an incorrect magnon spectrum, and spurious symmetry-protected topological magnon degeneracies can occur [26]. Often, these omitted anisotropic terms are actually what break additional symmetries and split otherwise degenerate magnon bands [3, 26, 34]. This phenomena can be corrected by going to higher order spin wave theory or real-space perturbation theory, or more fundamentally we can derive the bonds full exchange tensor allowed by the symmetry of the lattice. If the correct symmetries for each bond are identified, we can apply them to LSWT from the beginning, avoiding any errors coming from the omissions, and LSWT will respect the real degeneracy-lifting anisotropies of the material. Shell anomalies and anisotropy blindness may even jointly take affect in a material, meaning appropriate symmetry analysis would be essential for modelling.

Conventional ferromagnets have one spin sublattice, nonzero magnetisation, have spin splitting in bands, and broken time-reversal (T) symmetry (involving flipping of spins). Antiferromagnets have two sublattices with opposite spin linked by a translation or inversion, zero net magnetisation, and T-invariant, spin-degenerate bands. Contrary to both, there are recently discovered altermagnetic materials exhibit zero net magnetisation but have alternating spin-splitting in bands that breaks T symmetry [35, 36]. Altermagnets have opposite spin sublattices, linked by a rotation, rather than inversion or translation. Altermagnets could have many implications in spintronics, superconductivity and other fields [35–37]. Group theory provides the framework for describing altermagnetism and its properties, and the space-group of a material can help identify a possible altermagnetic candidate using the identification rules formulated with their discovery [35, 36]. Also, the splitting of magnon bands as a result of correcting a shell anomaly in antiferromagnets is identical to phenomena reported in altermagnets [26, 35, 36]. The project can be used to identify possible altermagnetic structures by verifying if two sublattices are connected by a rotation, and by resolving shell anomalies in antiferromagnets.

SpinW is a MATLAB library used to simulate magnetic structures and solve spin Hamiltonians using LSWT [13, 38]. It shows the use in automating these processes, and simplifies otherwise tedious calculations. However, it has been noted that SpinW can lead to incorrect results when compared to methodically calculated solutions [39]. This gives another reason to provide a robust process for obtaining the correct form of exchange tensor so it can be used in further research without fear of inaccuracy.

In this project, the algorithm developed has proved its capability of finding the allowed components of the Heisenberg Hamiltonian exchange tensor for any bond in a magnetic structure, and finding if bonds are symmetrically distinct. This is seen from tests on a structure of low symmetry, where it catches anisotropy blindness omissions and resolves the shell anomaly. The correct NN-bonds for the nonsymmorphic diamond structure were found, showing its capacity for handling non-trivial symmetry operations. Individual bonds in MnF_2 and $Y_3Fe_5O_{12}$ have been examined, resolving shell anomalies and showing allowed couplings such as DMI. MnF_2 has also been checked for altermagnetic candidacy by verifying that the sublattices are connected by a rotation, providing a tool to be used in the search for altermagnets. Mn_5Ge_3 has also been analysed, showing bonds capable of DMI and other anisotropic interactions, responsible for magnon propagation, relevant for the advancement of spintronic devices.

II. METHODS

A. Theory

Here the method for finding the symmetry allowed exchange tensor $\mathbf{J}_{ij}$ for any bond is laid out, along with the method to check if two bonds are in the same orbital X, therefore having the same independent tensor components, and to see how these tensors are related.

Firstly we start with the lattice, which in any material is described by three primitive lattice vectors. These vectors ensure that there is one lattice site per integer translation along one of these vectors, allowing us to describe atoms positions in each lattice site with fractional coordinates $\mathbf{A}$ in the range $0 \leq \mathbf{A} < 1$. The lattice forms a topological surface, meaning if one traverses any axis past the fractional coordinate of 1, they loop back around to the start of that cell at fractional coordinate 0. This is why points are invariant up to integer

lattice translations.

Atoms are positioned in the lattice, and the bonds between these atoms span the lattice. The bonds must respect all or a subset of symmetries that the lattice itself posses. Some operations might not leave the bond invariant, and so are not a symmetry of the bond, and cannot be used to specify its exchange tensor. Some operations could leave the bond invariant directly, meaning the bond preserves its direction. Some operations could leave the bond invariant but swap the endpoints, reversing its direction. Each bond has an energy contribution

$$E_{ij} = \mathbf{S}_i \cdot \mathbf{J}_{ij} \cdot \mathbf{S}_j, \tag{19}$$

where $\mathbf{S}_i$ and $\mathbf{S}_j$ are the two spin vectors at each end of the bond and $\mathbf{J}_{ij}$ is the exchange tensor. As any operation in the stabilizer group of the bond is also contained in the space-group of the crystal, it therefore leaves both the bond and the crystal unchanged. This means that the energy E_{ij} associated with that bond must also remain unchanged under that operation. Imposing this invariance on E_{ij} is what enforces the symmetry constraints on $\mathbf{J}_{ij}$, as by Eq. (19). Since the Hamiltonian in Eq. (1) sums over unordered pairs of spins, operations that swap the two sites (reverse the bond) must obey the same invariance condition on the energy. This results in the transpose of the exchange tensor $\mathbf{J}_{ij}^T$ being invariant under the reversing symmetry operation. We use all operations that leave the bond directly or in reverse to specify $\mathbf{J}_{ij}$ for the bond.

If a symmetry operation S does not leave a bond invariant, it moves it to another bond in the same orbit X [17]. The full Hamiltonian (Eq. 1) including every bond must be invariant under S. When a bond is rotated to another with S, the total sum of H does not change, and therefore these terms have to match, giving an equivalency between the two bond's exchange tensors. This is why bonds that can be mapped to one another share identical exchange tensor components, and why we can relate them in the algorithm.

If two bonds $(i-j)$, $(k-l)$ have different point groups $\mathbf{P}_{ij} \neq \mathbf{P}_{kl}$, which can be found from their stabilizer groups $\mathbf{G}_{ij}$ and $\mathbf{G}_{kl}$, they must lie in different orbits $X_{ij} \neq X_{kl}$ [17]. This means that they cannot be mapped to one another using any $S \in \mathbf{G}$, and is a way to verify that the two bonds carry exchange tensors with unique components.

B. Algorithm

A lattice is represented by matrix $\mathrm{L} = (\mathbf{a}_1\ \mathbf{a}_2\ \mathbf{a}_3)^{\mathrm{T}}$, where $\mathbf{a}_1$, $\mathbf{a}_2$, $\mathbf{a}_3$ represent the primitive lattice (column) vectors that define the unit cell of L. Each primitive lattice vector is defined by Cartesian coordinates $\mathbf{a}_i = (x_i, y_i, z_i)$. A vector $\mathbf{X} = f_1\mathbf{a}_1 + f_2\mathbf{a}_2 + f_3\mathbf{a}_3$, $f_i \in \mathbb{Q}$ can access any point (x, y, z) in the lattice, with the fractional coordinate of a point given by $\mathbf{A} = (f_1,\ f_2,\ f_3)$. Fractional coordinates $\mathbf{A}$ in the unit cell are in the range $[0, 1[$, and are related to Cartesian coordinates $\mathbf{X}$ with $\mathbf{X} = \mathrm{L}^{\mathrm{T}} \cdot \mathbf{A}$. $\mathbf{A}_u$ represents the fractional positions of the atoms in the unit cell with atomic numbers $\mathbf{n}_u$.

A supercell is created in order to look at bonds that are larger than the unit cell. An atom is selected at site i and an opposing atom is selected at site j, and these atoms form the endpoints of the bond. The process has been automated so that it is possible to loop through all possible sites j in the supercell and check the symmetries of each bond automatically.

Each atom at sites i and j have position vectors $\mathbf{A}_i$, $\mathbf{X}_i$ and $\mathbf{A}_j$, $\mathbf{X}_j$ respectively. The bond vectors are calculated as $\mathbf{K}_{ij} = \mathbf{X}_j - \mathbf{X}_i$. The norm $||\mathbf{K}_{ij}|| = d_{ij}$ gives the distance between $\mathbf{X}_i$ and $\mathbf{X}_j$. It is essential that d_{ij} is calculated in Cartesian coordinates, as these measure real distance in space, whereas fractional coordinates measure distances relative to the unit cell and can be distorted. If atoms $\mathbf{A}_j$ only within a certain distance of $\mathbf{A}_i$ need to be examined, atoms with distances from $\mathbf{A}_i$ larger than a chosen radius $r < d_{ij}$ are discarded. Each $\mathbf{A}_j$ is then sorted and grouped into shells p_{ij} based on d_{ij}.

The space group $\mathbf{G}$ of L consists of symmetry operations $S = (\mathrm{R}, \mathbf{T}) \in \mathbf{G}$, where R is a symmetry element matrix, each paired with a translation $\mathbf{T}$. $\mathbf{G}$ is found given $\mathbf{a}_i$, $\mathbf{A}_u$ and $\mathbf{n}_u$. The symmetry operations that leave the bond $\mathbf{B}_{ij} = \mathbf{A}_j - \mathbf{A}_i$ invariant are needed to specify the exchange tensor $\mathbf{J}_{ij}$. These operations form the stabilizer group $\mathbf{G}_{ij}$ of the bond.

The algorithm to find each symmetry operation in the stabilizer group of the bond $S \in \mathbf{G}_{ij}$, so that $\mathbf{B}_{ij} = S\mathbf{B}_{ij} = \mathrm{R}\mathbf{B}_{ij} + \mathbf{T}$, and to specify the tensor $\mathbf{J}_{ij}$ associated with the bond is as follows. Loop over all $S \in \mathbf{G}$ and apply the symmetry operation S to the endpoints of the bond, $\mathbf{A}'_i = S\mathbf{A}_i$ and $\mathbf{A}'_j = S\mathbf{A}_j$. The operation on the atoms at sites i, j has placed the atoms at sites i', j'. Apply a modulus operation to the atom at site i', $\mathbf{U}'_i = \mathbf{A}'_i \bmod 1$, yielding a value in the range $[0, 1[$ to give the equivalent of the operated point in the unit cell. Also, apply the modulo operation to the point at site i, $\mathbf{U}_i = \mathbf{A}_i \bmod 1$ to verify its position in the unit cell. If the point at site i' is equal to the point at site i when both are transformed to the unit cell, $\mathbf{U}'_i = \mathbf{U}_i$, the positions are invariant accounting for integer lattice translations, and we continue. The vector from site i to site i', $\Delta\mathbf{A}_i = \mathbf{A}'_i - \mathbf{A}_i$, is calculated to see how the atom has transformed. If the atom at site j' is translated back to site j when the same translation is applied, $\mathbf{A}'_j - \Delta\mathbf{A}_i = \mathbf{A}_j$, then both endpoints in the bond have been transformed in the same way, and the bond has been left invariant directly. The matrix element R of S can be stored as a direct point group operation in the set $\boldsymbol{O}_D$. S is also stored in the stabilizer group $\mathbf{G}_{ij}$

Alternatively, if the position of the endpoint at site i' does not equal the position of the endpoint at site i accounting for integer lattice translations $\mathbf{U}'_i \neq \mathbf{U}_i$, then we find the position of $\mathbf{A}'_j$ in the unit cell $\mathbf{U}'_j = \mathbf{A}'_j \bmod 1$. If the operated point at site j' equals the endpoint at site i accounting for integer lattice translations $\mathbf{U}'_j = \mathbf{U}_i$, then $\mathbf{A}'_j$ and $\mathbf{A}_i$ are invariant, and we continue to check if the operation reverses the bond. The vector between these points $\Delta\mathbf{A}'_{ij} = \mathbf{A}'_j - \mathbf{A}_i$ is found. If

$\mathbf{A}'_i - \Delta\mathbf{A}_{ij} = \mathbf{A}_j$, then the endpoints have swapped positions. The symmetry operation S has reversed the bond and R is stored as a reversal operation in the set $\boldsymbol{O}_R$. S is again stored in stabilizer group $\mathbf{G}_{ij}$.

$\mathbf{J}_{ij}$ represents the exchange interaction tensor between atoms $\mathbf{A}_i$ and $\mathbf{A}_j$ at sites i and j. $\mathbf{J}_{ij}$ is firstly initialised unspecified with all components allowed. To specify, loop over each $\mathrm{R} \in O_D$ and apply the operations in the form

$$\mathbf{J}_{ij} = \mathrm{R} \cdot \mathbf{J}_{ij} \cdot \mathrm{R}^T \quad (\forall \mathrm{R} \in O_D). \tag{20}$$

This provides a set of simultaneous equations that reduce the number of allowed components of $\mathbf{J}_{ij}$. Substitute the results in to $\mathbf{J}_{ij}$. Next, loop over each $\mathrm{R} \in O_R$ and apply in the form

$$\mathbf{J}_{ij} = \mathbf{J}_{ji}^T = (\mathrm{R} \cdot \mathbf{J}_{ij} \cdot \mathrm{R}^T)^T \quad (\forall \mathrm{R} \in O_R). \tag{21}$$

This again provides a set of simultaneous equations that further reduce the number of allowed components of $\mathbf{J}_{ij}$. The stabilizer group $\mathbf{G}_{ij}$ of the bond has been found, and again, to obtain the point group $\mathbf{P}_{ij}$ of the bond we take all $S \in \mathbf{G}_{ij}$ and set all translations to $\mathbf{0}$, $\mathbf{P}_{ij} = \{S \in \mathbf{G}_{ij}, S = (\mathrm{R}, \mathbf{T} = \mathbf{0})\}$. The specified $\mathbf{J}_{ij}$ is then returned with bond vector $\mathbf{B}_{ij}, \mathbf{K}_{ij}$, starting position $\mathbf{A}_i, \mathbf{X}_i$, and point group $\mathbf{P}_{ij}$.

If atoms $\mathbf{A}_i$, $\mathbf{A}_j$ with atomic numbers n_i, n_j form a bond $\mathbf{B}_{ij}$ with distance d_{ij}, and atoms $\mathbf{A}_k$, $\mathbf{A}_l$ with equivalent atomic numbers $n_k = n_i$, $n_l = n_j$ form bond $\mathbf{B}_{kl}$ between sites k and l with distance $d_{kl} = d_{ij}$, we can try to relate the components of their exchange tensors $\mathbf{J}_{ij}, \mathbf{J}_{kl}$. If $\mathbf{B}_{ij}$ can be mapped on to $\mathbf{B}_{kl}$ by a space group operation S, that is if $\mathbf{B}_{kl} = S\mathbf{B}_{ij} = \mathrm{R}\mathbf{B}_{ij} + \mathbf{T}$, the tensor components are related in the form

$$\mathbf{J}_{kl} = \mathrm{R} \cdot \mathbf{J}_{ij} \cdot \mathrm{R}^T, \tag{22}$$

where R is the matrix element of S. To find a space group operation that maps the bonds, we employ a similar method as before. Loop over all $S \in \mathbf{G}$ and apply the symmetry operation to the endpoints of the bond between sites i and j, $\mathbf{A}'_i = S\mathbf{A}_i$ and $\mathbf{A}'_j = S\mathbf{A}_j$. Apply a modulus operation to the endpoint at site k, $\mathbf{U}_k = \mathbf{A}_k \bmod 1$, and the transformed endpoints at sites i' and j', $\mathbf{U}'_i = \mathbf{A}'_i \bmod 1$, $\mathbf{U}'_j = \mathbf{A}'_j \bmod 1$. If $\mathbf{U}'_i = \mathbf{U}_k$, then the points are invariant accounting for integer lattice translations, and we continue. The vector from the atom at site i' to the atom at site k is computed $\Delta\mathbf{A}'_{ik} = \mathbf{A}'_i - \mathbf{A}_k$. If the same translation takes the atom on site j to site l, $\mathbf{A}'_j - \Delta\mathbf{A}'_{ik} = \mathbf{A}_l$, then the operation S has mapped $\mathbf{B}_{ij}$ on to $\mathbf{B}_{kl}$, and R can be used in Eq. (22) to find the corresponding tensor.

Again, if $\mathbf{U}'_i \neq \mathbf{U}_k$, we check with to see if $\mathbf{A}_k$ is invariant with $\mathbf{A}'_j$. If $\mathbf{U}'_j = \mathbf{U}_k$, then the points are invariant and we proceed to check if S maps $\mathbf{B}_{ij}$ to $\mathbf{B}_{kl}$ in reverse. The vector form the atom at site j' to the atom at site k $\Delta\mathbf{A}'_{jk} = \mathbf{A}'_j - \mathbf{A}_k$ is found. If $\mathbf{A}'_l - \Delta\mathbf{A}'_{jk} = \mathbf{A}_l$, S has mapped the bond in reverse, and we use

$$\mathbf{J}_{kl} = (\mathbf{J}_{lk})^T = (\mathrm{R} \cdot \mathbf{J}_{ij} \cdot \mathrm{R}^T)^T. \tag{23}$$

to relate the tensors of the two bonds. S is again stored in the orbit group X_{ij}. Only the symmetry element from one symmetry operation that maps the bond in either form is necessary to give $\mathbf{J}_{kl}$ from $\mathbf{J}_{ij}$. If the bonds have been mapped directly or in reverse, they are in the same orbit X, and S is stored in the orbit group X_{ij}. Every bond in an particular orbit X is symmetry equivalent and must share the same independent tensor entries.

C. General Details of the Code

The code was written in Python 3.12 [40]. Material details were taken from Materials Project [41, 42] and imported as .cif files. Files were read using the Atomic Simulation Environment (ASE) package [43], and the data was converted into an atoms object. A supercell was built using ASE. The lattice matrix L, fractional positions $\mathbf{A}_u$, Cartesian positions $\mathbf{X}_u$ and numbers n_u were extracted from the atoms object. Spglib [44] was used to find the space group $\mathbf{G}$ and symmetry operations S of the crystal. The symmetry operations were organised as a Python class. The SymPy package [45] was used to express the undetermined symbolic exchange tensor $\mathbf{J}_{ij}$, and SymPy was essential for carrying out the symbolic mathematics required in this project. Simultaneous equations were acquired from Eqs. (20) and (21), and solved using the SymPy solvers module. Spglib was used to find a point group given the symmetry operation matrices. NumPy [46] was used extensively for array handling and calculations. Plots were generated using Matplotlib [47].

III. RESULTS

A. Tests

The code has been rigorously tested on lattice models with varying symmetries, and the results confirm both the accuracy of its calculations and the robustness of the implementation. The paper [26] was instrumental for the motivation of this project, and a scenario is laid out in this paper that describes a situation of geometry on a ferromagnetic lattice that has highly anisotropic couplings which one could find in an insulating magnet with strong SOC. LSWT on this model exhibits both a shell anomaly and anisotropy blindness, giving a perfect example to test the code built for the project and show that it avoids these errors.

We have a tetragonal lattice as seen in Fig. (3) with primitive lattice vectors

$$\mathbf{a}_1 = (a, 0, 0),\ \mathbf{a}_2 = (0, a, 0),\ \mathbf{a}_3 = (0, 0, c), \tag{24}$$

which lie along the x, y and z axis respectively, as the cell is orthogonal. a and c are lattice constants. The atoms in this

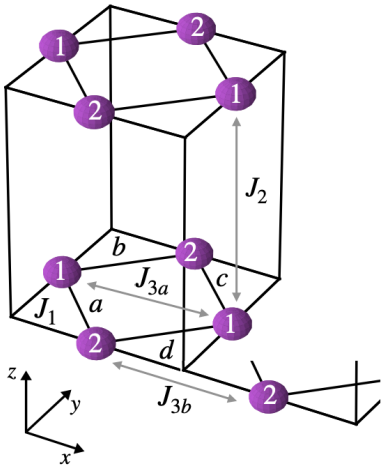

FIG. 3: Tetragonal lattice model with bonds labelled out to the third shell. First shell bonds labelled a, b, c, d. The circles labelled $1, 2$ represent $\mathbf{A}_1, \mathbf{A}_2$ and the positions a lattice translation away in Eq. (25). Figure taken from [26].

model take positions:

$$\begin{aligned} &\mathbf{A}_1 = (0, 1/2, z), \mathbf{A}_2 = (1/2, 0, z), \\ &\mathbf{A}_{1x} = \mathbf{A}_1 + \mathbf{a}_1, \mathbf{A}_{1y} = \mathbf{A}_1 + \mathbf{a}_2, \\ &\mathbf{A}_{1z} = \mathbf{A}_1 + \mathbf{a}_3, \mathbf{A}_{2x} = \mathbf{A}_2 + \mathbf{a}_1, \\ &\mathbf{A}_{2y} = \mathbf{A}_2 + \mathbf{a}_2, \mathbf{A}_{2z} = \mathbf{A}_2 + \mathbf{a}_3, \end{aligned} \tag{25}$$

where each atom is represented by a fractional coordinate $\mathbf{A}_i$. The fractional value of primitive lattice vectors are added to positions $\mathbf{A}_1$ and $\mathbf{A}_2$ to give the neighbouring atoms positions (see Fig. 3).

The structure has the symmorphic space group $P4$, consisting of the three primitive lattice translations and four point-group operations; the identity E, a two-fold (180°) rotation around the z-axis C_{2z}, and positive and negative four-fold (90°) rotations around the z-axis, C_{4z}^+ and C_{4z}^-, represented with matrices

$$\begin{aligned} E &= \begin{pmatrix} 1 & 0 & 0 \\ 0 & 1 & 0 \\ 0 & 0 & 1 \end{pmatrix}, \quad C_{2z} = \begin{pmatrix} -1 & 0 & 0 \\ 0 & -1 & 0 \\ 0 & 0 & 1 \end{pmatrix}, \\ C_{4z}^+ &= \begin{pmatrix} 0 & -1 & 0 \\ 1 & 0 & 0 \\ 0 & 0 & 1 \end{pmatrix}, \quad C_{4z}^- = \begin{pmatrix} 0 & 1 & 0 \\ -1 & 0 & 0 \\ 0 & 0 & 1 \end{pmatrix}. \end{aligned} \tag{26}$$

In [26] four separate couplings are set for bonds labelled in Fig. (3):

$$\begin{aligned} &\mathbf{J}_1 : (\mathbf{A}_1, \mathbf{A}_2)_a, (\mathbf{A}_1, \mathbf{A}_{2y})_b, \\ &(\mathbf{A}_{1x}, \mathbf{A}_{2y})_c, (\mathbf{A}_{1x}, \mathbf{A}_2)_d \,, \end{aligned} \tag{27}$$

$$\mathbf{J}_2 : (\mathbf{A}_1, \mathbf{A}_{1z})_e, (\mathbf{A}_2, \mathbf{A}_{2z})_f, \tag{28}$$

$$\mathbf{J}_{3a} : (\mathbf{A}_1, \mathbf{A}_{1x})_g, (\mathbf{A}_2, \mathbf{A}_{2y})_h \,, \tag{29}$$

$$\mathbf{J}_{3b} : (\mathbf{A}_1, \mathbf{A}_{1y})_i, (\mathbf{A}_2, \mathbf{A}_{2x})_j. \tag{30}$$

where the positions in brackets represent the endpoints of the bond, and the subscript is the bond label.

We need to verify that these couplings are indeed symmetrically independent, and the components of the tensors that are allowed by symmetry. Starting with bond a in the first shell first shell with tensor $\mathbf{J}_1(a)$, we check if any symmetry operation in the space group leaves the bond invariant using the algorithm. The only operation that leaves a invariant is the identity E, in the set O_D. E can be applied to $\mathbf{J}_1(a)$ using Eq. (20), obviously leaving $\mathbf{J}_1(a)$ unchanged. Therefore $\mathbf{J}_{1a}$ still contains 9 independent components:

$$\mathbf{J}_1(a) = \begin{pmatrix} J_1^{xx} & J_1^{xy} & J_1^{xz} \\ J_1^{yx} & J_1^{yy} & J_1^{yz} \\ J_1^{zx} & J_1^{zy} & J_1^{zz} \end{pmatrix}, \tag{31}$$

and this is in agreement with the result in the paper. Now we use the algorithm to find if bond b, c, d can be mapped to from a. We find that the bonds are mapped with the following operations:

$$b = C_{4z}^- \cdot a \quad \{C_{4z}^- \in O_R\}, \tag{32}$$

$$c = C_{2z} \cdot a \quad \{C_{2z} \in O_D\}, \tag{33}$$

$$d = C_{4z}^+ \cdot a \quad \{C_{4z}^+ \in O_D\}. \tag{34}$$

This confirms that the bonds all share the same tensor components. When then use these symmetry elements to find the corresponding tensors for each bond using equations (22) and (23), yielding

$$\mathbf{J}_1(b) = \begin{pmatrix} J_1^{yy} & -J_1^{xy} & J_1^{zy} \\ -J_1^{yx} & J_1^{xx} & -J_1^{zx} \\ J_1^{yz} & -J_1^{xz} & J_1^{zz} \end{pmatrix}, \tag{35}$$

$$\mathbf{J}_1(c) = \begin{pmatrix} J_1^{xx} & J_1^{xy} & -J_1^{xz} \\ J_1^{yx} & J_1^{yy} & -J_1^{yz} \\ -J_1^{zx} & -J_1^{zy} & J_1^{zz} \end{pmatrix}, \tag{36}$$

$$\mathbf{J}_1(d) = \begin{pmatrix} J_1^{yy} & -J_1^{xy} & -J_1^{zy} \\ -J_1^{yx} & J_1^{xx} & J_1^{yz} \\ -J_1^{yz} & J_1^{xz} & J_1^{zz} \end{pmatrix}, \tag{37}$$

and all of these tensors are in agreement with the results in [26].

We now go to the next shell, and calculate the allowed tensor components for the bonds that run along the z-axis. We initialise bond e with tensor $\mathbf{J}_2(e)$, and specify using the algorithm. The set of operations that directly leave e invariant

consists of the identity E and C_{2z}. No operation in the space group reverses the bond. This gives

$$\mathbf{J}_2(e) = \begin{pmatrix} J_2^{xx} & J_2^{xy} & 0 \\ J_2^{yx} & J_2^{yy} & 0 \\ 0 & 0 & J_2^{zz} \end{pmatrix}, \tag{38}$$

with 5 independent components. We then check if e can be mapped to f, and it is possible in the following ways:

$$\begin{aligned} f &= C_{4z}^{+} \cdot e \quad \{C_{4z}^{+} \in O_D\}, \\ f &= C_{4z}^{-} \cdot e \quad \{C_{4z}^{-} \in O_D\}, \end{aligned} \tag{39}$$

which gives

$$\mathbf{J}_2(f) = \begin{pmatrix} J_2^{yy} & -J_2^{yx} & 0 \\ -J_2^{xy} & J_2^{xx} & 0 \\ 0 & 0 & J_2^{zz} \end{pmatrix}, \tag{40}$$

and both of these results are in agreement with [26]. We can see from the allowed components that these bonds can only exhibit antisymmetric coupling between the x and y components.

Finally, we examine the third shell, in which the shell anomaly takes place. We start with $\mathbf{J}_{3a}(g)$ on bond g and specify using the algorithm. Apart from E, only the operation C_{2z} can be used to specify $\mathbf{J}_{3a}(g)$ which reverses g. This gives a tensor with 6 independent components;

$$\mathbf{J}_{3a}(g) = \begin{pmatrix} J_{3a}^{xx} & J_{3a}^{xy} & -J_{3a}^{zx} \\ J_{3a}^{yx} & J_{3a}^{yy} & -J_{3a}^{zy} \\ J_{3a}^{zx} & J_{3a}^{zy} & J_{3a}^{zz} \end{pmatrix}, \tag{41}$$

which has the same equivalencies as the result in [26]. We see that antisymmetric exchange $\mathbf{D}_{ij}$ is permitted on this bond. The algorithm then confirms that g can be mapped to h in two ways:

$$\begin{aligned} h &= C_{4z}^{+} \cdot g \quad \{C_{4z}^{+} \in O_D\}, \\ h^T &= C_{4z}^{-} \cdot g \quad \{C_{4z}^{-} \in O_R\}, \end{aligned} \tag{42}$$

which gives the tensor for h;

$$\mathbf{J}_{3a}(h) = \begin{pmatrix} J_{3a}^{yy} & -J_{3a}^{yx} & J_{3a}^{zy} \\ -J_{3a}^{yx} & J_{3a}^{yy} & -J_{3a}^{zx} \\ -J_{3a}^{zy} & J_{3a}^{zx} & J_{3a}^{zz} \end{pmatrix}, \tag{43}$$

and confirms that bonds i, k cannot be reached from g using any of the space-group operations of the lattice. This confirms the shell anomaly and imposes two unique exchange tensors in the third shell of the lattice. The final tensor to check is initialised on bond i as $\mathbf{J}_3(i)$. The algorithm finds the bond invariant under E and C_{2z}, which reverses the bond. The resulting tensor is

$$\mathbf{J}_{3b}(i) = \begin{pmatrix} J_{3b}^{xx} & J_{3b}^{yx} & -J_{3b}^{zx} \\ J_{3b}^{yx} & J_{3b}^{yy} & -J_{3b}^{zy} \\ J_{3b}^{zx} & J_{3b}^{zy} & J_{3b}^{zz} \end{pmatrix}, \tag{44}$$

which has the same symmetry as $\mathbf{J}_{3a}(g)$, but all 6 components are completely independent of $\mathbf{J}_{3a}(g)$. The algorithm then finds that i can be mapped to j with

$$\begin{aligned} j &= C_{4z}^{-} \cdot i \quad \{C_{4z}^{+} \in O_D\}, \\ j^T &= C_{4z}^{+} \cdot i \quad \{C_{4z}^{-} \in O_R\}, \end{aligned} \tag{45}$$

and choosing the rotation C_{4z}^{-} to find $\mathbf{J}_{3b}(j)$ with Eq. (22), we obtain

$$\mathbf{J}_{3b}(j) = \begin{pmatrix} J_{3b}^{yy} & -J_{3b}^{yx} & -J_{3b}^{zy} \\ -J_{3b}^{yx} & J_{3b}^{xx} & -J_{3b}^{zx} \\ J_{3b}^{zy} & -J_{3b}^{zx} & J_{3b}^{zz} \end{pmatrix}, \tag{46}$$

which again has the same equivalencies reported in [26]. Consequently, the code has replicated all the results of the solution, and is verified to give correct calculations. In total, up to the third-neighbour shell our symmetry analysis permits $9 + 5 + 6 + 6 = 26$ independent exchange couplings, whereas a conventional LSWT model would include only 18 due to anisotropy blindness. If the third shell had a non-zero contribution to the exchange energy but was not included, a shell anomaly would be present in this structure, and LSWT would give the Hamiltonian a heightened symmetry [26]. This is avoided by calculating the symmetry allowed components for the independent bonds in the third shell, and the test has demonstrated that the algorithm does this accurately, providing a method for eliminating anisotropy blindness and shell anomalies in spin-wave calculations.

The code has also been tested on the more complex nonsymmorphic diamond cubic structure (seen in Fig. (4)) to check if it correctly handles symmetry operations including an intrinsic translation. This example is given in [48], and is to find the nearest-neighbour exchange constants. The first a bond has atomic positions $\mathbf{A}_i = (0, 0, 0)$ and $\mathbf{A}_j = (a/4, a/4, a/4)$ as endpoints, where a is the lattice constant for all cube edges. The solution shows exchange tensor

$$\mathbf{J}_1^{sol}(a) = \begin{pmatrix} \alpha & \beta & \beta \\ \beta & \alpha & \beta \\ \beta & \beta & \alpha \end{pmatrix}, \tag{47}$$

where α and β is the notation used in [48] to expresses clearly that there are 2 independent exchange constants involved with the bond.

We now use the algorithm to find the allowed exchange tensor for bond a starting with unspecified tensor $\mathbf{J}_1(a)$ then comparing with $\mathbf{J}_1^{sol}(a)$. First the symmetry operations S that

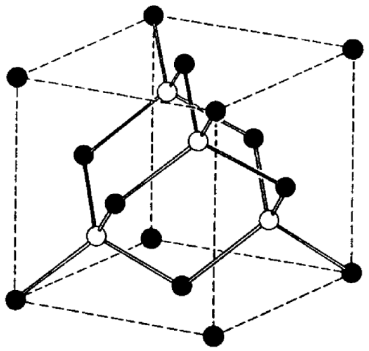

FIG. 4: Diamond cubic structure with space group $Fd3m$ consisting of two interpenetrating FCC lattices of cube edge a [48]. Each atom connects to 4 others in the first shell. Figure taken from [14].

leave a invariant were calculated, and the results show 8 such operations, of which 4 leave the bond directly invariant and 4 reverse the bond. Each $S \in O_D$ contains no intrinsic translation $\mathbf{T} = 0$ and are given by,

$$S_{D_1}(a) = \mathrm{R}_{D_1}(a) = \begin{pmatrix} 1 & 0 & 0 \\ 0 & 1 & 0 \\ 0 & 0 & 1 \end{pmatrix}, \tag{48}$$

$$S_{D_2}(a) = \mathrm{R}_{D_2}(a) = \begin{pmatrix} 1 & 0 & 0 \\ 0 & 0 & 1 \\ 0 & 1 & 0 \end{pmatrix}, \tag{49}$$

$$S_{D_3}(a) = \mathrm{R}_{D_3}(a) = \begin{pmatrix} 0 & 0 & 1 \\ 0 & 1 & 0 \\ 1 & 0 & 0 \end{pmatrix}, \tag{50}$$

$$S_{D_4}(a) = \mathrm{R}_{D_4}(a) = \begin{pmatrix} 0 & 1 & 0 \\ 1 & 0 & 0 \\ 0 & 0 & 1 \end{pmatrix}, \tag{51}$$

$$\{\mathrm{R}_{D_1}(a),\ \mathrm{R}_{D_2}(a),\ \mathrm{R}_{D_3}(a),\ \mathrm{R}_{D_4}(a)\ \in O_D\}. \tag{52}$$

These symmetry operations are applied to unspecified tensor $\mathbf{J}_1(a)$ using Eq. (20). The rest are compound operations that contain a symmetry element R and a translation along a quarter of the body diagonal $\mathbf{T}(a/4) = (a/4, a, 4, a, 4)$, giving

$$S_{R_1}(a) = (\mathrm{R}_{R_1}(a)|\mathbf{T}_{R_1}(a)) = \left(\begin{pmatrix} 0 & -1 & 0 \\ 0 & 0 & -1 \\ -1 & 0 & 0 \end{pmatrix} \,\middle|\, \mathbf{T}(a/4)\right), \tag{53}$$

$$S_{R_2}(a) = (\mathrm{R}_{R_2}(a)|\mathbf{T}_{R_2}(a)) = \left(\begin{pmatrix} -1 & 0 & 0 \\ 0 & 0 & -1 \\ 0 & -1 & 0 \end{pmatrix} \,\middle|\, \mathbf{T}(a/4)\right), \tag{54}$$

$$S_{R_3}(a) = (\mathrm{R}_{R_3}(a)|\mathbf{T}_{R_3}(a)) = \left(\begin{pmatrix} 0 & 0 & -1 \\ 0 & -1 & 0 \\ -1 & 0 & 0 \end{pmatrix} \,\middle|\, \mathbf{T}(a/4)\right), \tag{55}$$

$$S_{R_4}(a) = (\mathrm{R}_{R_4}(a)|\mathbf{T}_{R_4}(a)) = \left(\begin{pmatrix} 0 & -1 & 0 \\ -1 & 0 & 0 \\ 0 & 0 & -1 \end{pmatrix} \,\middle|\, \mathbf{T}(a/4)\right), \tag{56}$$

$$\{\mathrm{R}_{R_1}(a),\ \mathrm{R}_{R_2}(a),\ \mathrm{R}_{R_3}(a),\ \mathrm{R}_{R_4}(a)\ \in O_R\}. \tag{57}$$

These symmetry elements are further applied to $\mathbf{J}_1(a)$ using Eq. (21). In final form

$$\mathbf{J}_1(a) = \begin{pmatrix} J_1^{zz} & J_1^{zy} & J_1^{zy} \\ J_1^{zy} & J_1^{zz} & J_1^{zy} \\ J_1^{zy} & J_1^{zy} & J_1^{zz} \end{pmatrix}, \tag{58}$$

therefore

$$\mathbf{J}(a) = \mathbf{J}_{sol}(a), \tag{59}$$

and the algorithm has correctly identified the symmetry allowed couplings for the bond a. $\mathbf{J}_1(a)$ is purely symmetric, and if a magnetic material was to hold this structure, it would be prohibited from exhibiting antisymmetric exchange (DMI) on first neighbour bonds. We have shown that the algorithm is able to correctly specify a bond's tensor in a nonsymmorphic structure, handling compound operations.

We are now ready to find the exchange tensors for rest of the first shell bonds. Firstly we need to check if the bonds are related by symmetry, and therefore hold the same $\mathbf{J}_1$ components. The remaining bonds b, c and d in the first shell start from atom $\mathbf{A}_i$ and are to atomic positions $\mathbf{A}_k = (a/4, -a/4, -a/4)$, $\mathbf{A}_l = (-a/4, a/4, -a/4)$ and $\mathbf{A}_m = (-a/4, -a/4, a/4)$ respectively. Using the algorithm we find a can be mapped to the other bonds in many ways, and we are free to pick any operation. Choosing operations such that $S = (\mathrm{R}, \mathbf{0})$,

$$b = \mathrm{R}_{ab} \cdot a, \quad \mathrm{R}_{ab} = \begin{pmatrix} 1 & 0 & 0 \\ 0 & -1 & 0 \\ 0 & 0 & -1 \end{pmatrix}, \tag{60}$$

$$c = \mathrm{R}_{ac} \cdot a, \quad \mathrm{R}_{ac} = \begin{pmatrix} 0 & 0 & -1 \\ 0 & 1 & 0 \\ -1 & 0 & 0 \end{pmatrix}, \tag{61}$$

$$d = \mathrm{R}_{ad} \cdot a, \quad \mathrm{R}_{ad} = \begin{pmatrix} 0 & -1 & 0 \\ 0 & 0 & -1 \\ 1 & 0 & 0 \end{pmatrix}, \tag{62}$$

$$\{\mathrm{R}_{ab},\ \mathrm{R}_{ac},\ \mathrm{R}_{ad}\ \in O_D\}. \tag{63}$$

These elements are used to find the tensors for the corresponding bond from $\mathbf{J}_1(a)$ using Eq. (20), resulting in

$$\mathbf{J}_1(b) = \begin{pmatrix} J_1^{zz} & -J_1^{zy} & -J_1^{zy} \\ -J_1^{zy} & J_1^{zz} & J_1^{zy} \\ -J_1^{zy} & J_1^{zy} & J_1^{zz} \end{pmatrix}, \tag{64}$$

$$\mathbf{J}_1(c) = \begin{pmatrix} J_1^{zz} & -J_1^{zy} & J_1^{zy} \\ -J_1^{zy} & J_1^{zz} & -J_1^{zy} \\ J_1^{zy} & -J_1^{xy} & J_1^{zz} \end{pmatrix}, \tag{65}$$

$$\mathbf{J}_1(d) = \begin{pmatrix} J_1^{zz} & J_1^{zy} & -J_1^{zy} \\ J_1^{zy} & J_1^{zz} & -J_1^{zy} \\ -J_1^{zy} & -J_1^{xy} & J_1^{zz} \end{pmatrix}, \tag{66}$$

which are all in agreement with the solutions given in [48], showing the algorithm correctly identifies symmetry related exchanges. These tests have proved the algorithm to give correct calculations, and we can proceed to move on to real magnetic systems.

B. Application to Systems

Here we continue with the discussion on MnF_2 from the introduction, taken from [26]. Firstly, we can look at the bonds in the first shell characterised by the exchange coupling $\mathbf{J}_{bd}$ seen in Fig. [1]. All corner-to-centre bonds share the same point group m containing a mirror plane, and were confirmed to lie in the same orbital, as they can all be reached from one another using the space group operations of the lattice. Every bond shares coupling

$$\mathbf{J}_{bd} = \begin{pmatrix} J_{bd}^{yy} & J_{bd}^{yx} & J_{bd}^{yz} \\ J_{bd}^{yx} & J_{bd}^{yy} & J_{bd}^{yz} \\ J_{bd}^{zy} & J_{bd}^{zy} & J_{bd}^{zz} \end{pmatrix}, \tag{67}$$

which has exactly the same form when rotated to every other bond in the shell. The diagonal entries J_{bd}^{yy} and J_{bd}^{zz} set the preferred alignment of the spins. If $|J_{bd}^{zz}| > |J_{bd}^{yy}|$, z becomes the "easy" axis as it is harder to pull spins away from this direction [1]. The off-diagonal components $J_{bd}^{yx}, J_{bd}^{yz}, J_{bd}^{zy}$ mix spin fluctuations in different directions, which can produce direction-dependent magnon dispersion [30].

The corner-to-corner bonds d and d' with tensors $\mathbf{J}_d$ and $\mathbf{J}'_d$, seen in Fig. (1a) were attempted to be mapped using operations in the space group. Mapping was not possible and the bonds lie in different orbitals, meaning the bonds have distinct exchange tensors, proving the shell anomaly. $\mathbf{J}_d$ and $\mathbf{J}'_d$ were found to have the same form with equal point groups, meaning that it was necessary the use the algorithm to check if the bonds were symmetrically distinct, and not assume that they are equivalent because of their point groups. The information is displayed in Table. (I). Analysis gives

$$\mathbf{J}_d = \begin{pmatrix} J_d^{yy} & J_d^{yx} & 0 \\ J_d^{yx} & J_d^{yy} & 0 \\ 0 & 0 & J_d^{zz} \end{pmatrix}, \tag{68}$$

and

$$\mathbf{J}'_d = \begin{pmatrix} J_{d'}^{yy} & J_{d'}^{yx} & 0 \\ J_{d'}^{yx} & J_{d'}^{yy} & 0 \\ 0 & 0 & J_{d'}^{zz} \end{pmatrix}, \tag{69}$$

showing the equal form of both tensors. Again, the diagonal entries set preferred axis of alignment. DMI is forbidden on both tensors, so chiral textures cannot arise in the structure.

Coupling $\mathbf{J}_{ij}$	Distance (Å)	Point group $\mathbf{P}_{ij}$	No. unique components
$\mathbf{J}_{bd}$	3.8	m	5
$\mathbf{J}_d$	6.9	mmm	3
$\mathbf{J}'_d$	6.9	mmm	3

TABLE I: Unique MnF_2 bond exchange tensors with point groups and number of allowed components. Point groups given in Hermann-Mauguin notation [14]

By creating a supercell, the algorithm was used to examine how an Mn-F bond in one sublattice a is mapped to a Mn-F bond in sublattice b. The separate sublattices have opposite spin and are depicted by oppositely orientated polyhedra of F^- ions, seen in Fig. (1b). The bonds were mapped with symmetry operation

$$b = S_{ab} \cdot a \tag{70}$$

$$S_{ab} = (\mathrm{R}_{ab}|\mathbf{T}_{ab}) = \left(\begin{pmatrix} 0 & 1 & 0 \\ -1 & 0 & 0 \\ 0 & 0 & 1 \end{pmatrix} \;\middle|\; (\frac{\mathbf{1}}{\mathbf{2}}, \frac{\mathbf{1}}{\mathbf{2}}, \frac{\mathbf{1}}{\mathbf{2}}) \right), \tag{71}$$

which corresponds to a proper four-fold (90°) clockwise rotation $\mathrm{R}_{ab} = C_{4z}$ around the z-axis plus a translation $\mathbf{T}$ along half the body diagonal, given in fractional coordinates. The bond and rotation can be seen in Fig. (5). As the two opposite-spin sublattices are connect by a rotation, this satisfies the altermagnetic criteria and shows MnF_2 is a viable altermagnetic candidate [35, 36]. This results agrees with the band splitting reported from resolving the shell anomaly, anomalous to altermagnets. This approach could be used to analyse how opposite spin sublattices are connected in more structures to give possible altermagnetic candidates, helping research in spintronics [36].

An important result is one obtained for yttrium iron garnet (YIG, chemical formula $Y_3Fe_5O_{12}$). YIG is a ferrimagnetic material vital for understanding magnon dynamics and microwave magnetics. It can provide insight into these behaviours due to its extremely low magnetic damping and high Curie Temperature $T_c = 560$ K, meaning magnons are able to propagate over distances of centimetres and can be studied at room temperature. [10, 49, 50].

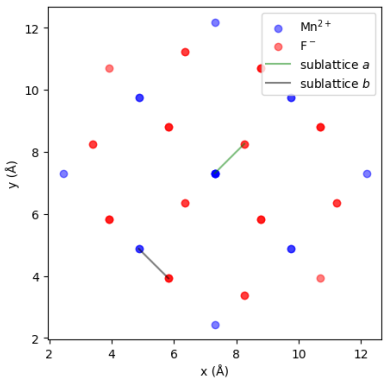

FIG. 5: Bonds on separate sublattices of MnF_2 connected by a C_{4z} rotation plus a translation along half the body diagonal.

Previous research into YIG assumed that third-nearest-neighbour (NN) bonds of equal length between the Fe^{3+} central ion, and each corner Fe^{3+} ion, share identical exchange parameters $\mathbf{J}_3$ [51]. However, more recent work [13] has shown that this assumption overlooks the differing symmetries of these bonds. Due to the surrounding environment of O^{-} and Y^{3+} ions, the bonds lying along the body diagonal of the unit cell exhibit higher symmetry than the other corner-to-centre bonds in the first octant of the unit cell [13], seen in Fig. (6). If considering just the magnetic lattice of Fe^{3+} ions, this structure posses a higher symmetry than the full lattice, and the space group of the full lattice must be used for an accurate symmetry analysis of the bonds.

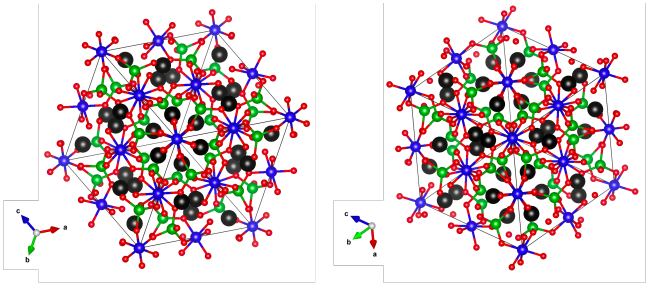

(a) (b)

FIG. 6: Unit cell of YIG. (a) View along the body-diagonal highlighting the highly symmetrical layout including a three-fold rotation around its axis. (b) View along a less symmetrical corner-to-centre bond with a two-fold rotation around its axis. Figures generated with VESTA [29].

The study [13] claims the NN bonds exhibits distinct exchange interactions labelled $\mathbf{J}_{3a}$ and $\mathbf{J}_{3b}$, as shown in Fig. (7). The algorithm confirmed that the bonds could not be mapped onto each other using any symmetry operation of the space group of the lattice, meaning they are in separate orbitals and are distinct. It was found that $\mathbf{J}_{3a}$ has point group 32, and $\mathbf{J}_{3b}$ has point group 2, confirming their independence. Information of the interactions is given in table [II]. Specification of $\mathbf{J}$ for each of the bonds clearly identifies two distinct exchange tensors with a differing number of allowed components;

Coupling $\mathbf{J}_{ij}$	Distance (Å)	Point group $\mathbf{P}_{ij}$	No. unique components
$\mathbf{J}_{3a}$	5.44	2	6
$\mathbf{J}_{3b}$	5.44	32	3

TABLE II: Unique $Y_3Fe_5O_{12}$ third-NN shell bond exchange tensors from [13] with point groups and number of allowed components. Point groups given in Hermann-Mauguin notation [14]

$$\mathbf{J}_{3b} = \begin{pmatrix} J_{3b}^{zz} & J_{3b}^{zx} & J_{3b}^{zy} \\ J_{3b}^{zy} & J_{3b}^{zz} & J_{3b}^{zx} \\ J_{3b}^{zx} & J_{3b}^{zy} & J_{3b}^{zz} \end{pmatrix}, \tag{72}$$

$$\mathbf{J}_{3a} = \begin{pmatrix} J_{3a}^{yy} & J_{3a}^{xy} & -J_{3a}^{zy} \\ J_{3a}^{yx} & J_{3a}^{yy} & -J_{3a}^{zx} \\ J_{3a}^{zx} & J_{3a}^{zy} & J_{3a}^{zz} \end{pmatrix}. \tag{73}$$

In $\mathbf{J}_{3b}$, the equal diagonal entries give isotropic exchange along each principal axis, while the symmetric off-diagonals J_{3b}^{zx} and J_{3b}^{zy} mix zx and zy fluctuations. The DMI vector $\mathbf{D}_{3b}$ vanishes, so no chirality is introduced. $\mathbf{J}_{3a}$ has a lower symmetry with more allowed couplings. J_{3b}^{yy} sets the energy cost tilt spins in the xy plane. The interaction can have symmetric anisotropic couplings, and can exhibit a 3D DMI vector with D_{3b}^{x} and D_{3b}^{y} constrained to be of equal length.

The symmetrical analysis has quickly confirmed that the two bonds are distinct, and given insight into the possible magnetic behaviour of YIG. This is an example how useful the algorithm can be to get results that have been overlooked in previous research [51]. The inequivalent bonds in the equal shell shows this was a case of a shell anomaly. It's clear to see how these can go unnoticed, and this rigorous approach to find local independent interactions can be used to find more symmetrically distinct bonds in materials that have not been precisely studied in the past.

Mn_5Ge_3 is a ferromagnetic material with Curie temperature $T_c = 296K$ [52], meaning it can hold spin-polarised currents around room temperature, making it an ideal candidate for spintronic devices. Mn_5Ge_3 has a centrosymmetric hexagonal structure, and contains zero net Dzyaloshinskii-Moriya interaction. Recent work has shown that topological magnons are enabled in Mn_5Ge_3 despite the lack of DMI, understood to be because of a lack of inversion symmetry at the bond level [3]. We can test this using the algorithm to find the allowed magnetic interactions on bonds in the material. Mn_5Ge_3 has space group $P6_3/mcm$, and the magnetic manganese ions have two symmetrically distinct positions labelled Mn1 and Mn2. The Mn1 ions form a hexagonal structure enclosing a honeycomb structure of Mn2 ions. The exchange interaction tensors have been calculated for each bonding shell (labelled in Fig. (8). Each bond in a NN-shell was found to be in the same orbital, so we can determine one form of exchange tensor for each.

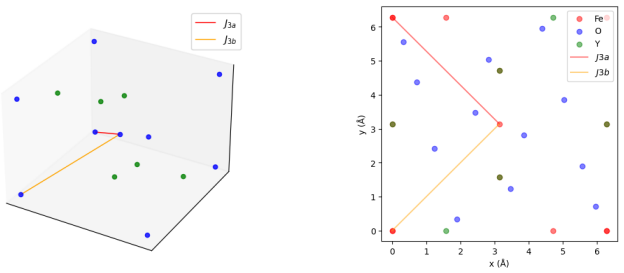

(a) (b)

FIG. 7: Crystal structure of the first octant of the unit cell of YIG. (a) Magnetic sublattice with Fe^{3+} octahedral sites in blue and tetrahedral sites in green [13]. $\mathbf{J}_{3b}$ lies along the body diagonal and accounts for two of the corner-to-centre bonds. $\mathbf{J}_{3a}$ has a lower symmetry and accounts for the other six bonds in the shell. (b) Top-down view highlighting the oxygen environment.

Starting from the second shell, the bond connects ions Mn1-Mn2 and has exchange tensor

$$\mathbf{J}_2 = \begin{pmatrix} J_2^{xx} & J_2^{xy} & J_2^{xz} \\ J_2^{yx} & J_2^{yy} & J_2^{yz} \\ J_2^{zx} & J_2^{zy} & J_2^{zz} \end{pmatrix}, \tag{74}$$

which shows there are no symmetry constraints. Both anisotropic and antisymmetric couplings are allowed. $\mathbf{D}_2$ is not constrained and can point in any direction. The three-dimensional DMI is responsible for opening topological gaps in the magnon bands as reported in [3]. The third shell connects bonds Mn2-Mn2 and has tensor

$$\mathbf{J}_3 = \begin{pmatrix} J_3^{xx} & J_3^{xy} & 0 \\ J_3^{yx} & J_3^{yy} & 0 \\ 0 & 0 & J_3^{zz} \end{pmatrix}, \tag{75}$$

so $\mathbf{J}_3$ is allowed to have non-zero $\mathbf{D}_3^z$ only, meaning the DMI is restricted to point in the z-direction. This is in agreement with [3], and the orientation of $\mathbf{D}_3$ on this bond can be seen in Fig. (8). By Eq. (2), this couples $\mathbf{S}_i^x$ with $\mathbf{S}_j^y$, meaning an x-fluctuation on spin i cants spin j in the y-direction, generating chiral spin textures in the xy plane. The fourth shell has bond Mn2-Mn2 that traverses the z-axis, with form

$$\mathbf{J}_4 = \begin{pmatrix} J_4^{xx} & J_4^{xy} & J_4^{xz} \\ J_4^{yx} & J_4^{yy} & J_4^{yz} \\ J_4^{zx} & J_4^{zy} & J_4^{zz} \end{pmatrix}. \tag{76}$$

All components survive in this tensor, meaning the bond is free to hold DMI or anisotropic exchange. For the fifth shell, we obtain a tensor of the form

$$\mathbf{J}_5 = \begin{pmatrix} J_5^{yy} & J_5^{yx} & J_5^{zy} \\ J_5^{yx} & J_5^{yy} & J_5^{zy} \\ J_5^{zy} & J_5^{zy} & J_5^{zz} \end{pmatrix}, \tag{77}$$

which is fully symmetric giving zero DMI, but anisotropic couplings can still remain.

This analysis has correctly identified possible DMI contributions localised on bonds as reported in [3], which are responsible for the topological stability of the magnons. The method has been proved useful for confirming the existence of localised DMI in Mn_5Ge_3, and can be put forward for on more magnetic materials to find DMI driven magnons for spintronic applications [10].

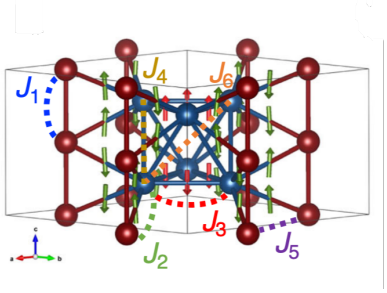

FIG. 8: Crystal structure of Mn_5Ge_3. Mn1 positions in red and Mn2 positions in blue. Exchange interaction tensors shown for the corresponding bonds in each shell. Orientation of DMI vectors shown on the bonds, restricted to the z-axis for $\mathbf{J}_3$, and free for $\mathbf{J}_2$. Figure taken from [3].

Finally, showing the tensors for the first and sixth shell in Mn_5Ge_3,

$$\mathbf{J}_1 = \begin{pmatrix} J_1^{yy} & \frac{J_1^{yy}}{2} & 0 \\ \frac{J_1^{yy}}{2} & J_1^{yy} & 0 \\ 0 & 0 & J_1^{zz} \end{pmatrix}, \tag{78}$$

$$\mathbf{J}_6 = \begin{pmatrix} 2J_6^{yx} & J_6^{yx} & 0 \\ J_6^{yx} & J_6^{yy} & J_6^{zy} \\ 0 & J_6^{zy} & J_6^{zz} \end{pmatrix}, \tag{79}$$

both seem to be completely symmetric and each have two components. However, the results contain constants, which have not previously appear in calculations. Looking into this further, it was found that some symmetry operations given by Spglib in the method are not orthogonal. These matrices are expressed in the fractional coordinate basis of the lattice. For example,

$$\mathrm{R}_1 = \begin{pmatrix} 0 & -1 & 0 \\ 1 & -1 & 0 \\ 0 & 0 & 1 \end{pmatrix} \tag{80}$$

is a symmetry operation of the first bond. Before applying this rotation to the exchange tensor in Eq. (20), a conversion to the

Cartesian basis using the lattice parameters must be done by

$$\mathrm{R}_{cart} = \mathrm{L} \cdot \mathrm{R}_{frac} \cdot \mathrm{L}^{T}, \tag{81}$$

as the exchange tensor is defined in the Cartesian basis. This could arise when crystals have non-orthogonal lattice basis vectors, and should be carefully handled when looking at structures such as this hexagonal Mn_5Ge_3. This was oversight in the of the application of the algorithm, and the method will be amended for future use.

IV. CONCLUSION

A. General remarks

The aim of this project was to automate the process of finding the allowed components of $\mathbf{J}_{ij}$. This has been achieved, however there was an issue of applying the incorrect form the symmetry operation in the lattice basis to $\mathbf{J}_{ij}$ in the Cartesian basis. The form of the matrices provided was not checked appropriately. As a third party software was used, it should have been studied rigorously to avoid such an oversight. This will be amended in the code, preparing it for future use. More tests should be done on structures with non-orthogonal lattice basis vectors. Anisotropic and Dzyaloshinskii-Moriya interactions were identified in Mn_5Ge_3, agreeing with experiment [3]. Despite this, it may be necessary to reanalyse each bond exchange contribution in Mn_5Ge_3 with this amendment of the method to have clarity of the findings. This would have been done if time were permitted to change the algorithm. Some point groups could also not be found due to a bug in the Spglib function that took in the symmetry matrices of the bond. These two issues could be related, and a thorough investigation should be had. An ulterior method could be use to obtain point groups going forward. Group theory has been proved useful and provided a vigorous method for specifying the tensors using Neumann's principle. The derived components or any magnetic material including longitudinal-transverse couplings can be used in LSWT, avoiding incorrect spin-wave predictions. Results from MnF_2 correctly derived symmetry distinct bonds proposed in [26], showing this algorithm can be put forward to test many systems suspected of shell anomalies, and aid research into altermagnetic structures if distinct further neighbour bonds are included in LSWT calculations, uncovering their characteristic spin-splitting in magnon bands [35, 36]. Research into $Y_3Fe_5O_{12}$ [13] has been backed up by finding symmetry distinct bonds in the third shell. The specific couplings found could provide insight for possible magnon formations aiding spintronic related discoveries [10]. The code has shown to be useful in different aspects of magnetic research, and there could be many more ways in which this group theory approach could be proved valuable to describe phenomena not discussed in this paper.

B. Possible Improvements of the Method

The current code could be improved by taking spin-space and time-reversal symmetries into account when applying space group operations to atoms along each bond. This would allow us to include magnetic space groups in the calculations, which is would be useful when studying materials like altermagnets.

Super-exchange is a mechanism where magnetic ions interact indirectly through non-magnetic atoms along the bond [1]. It is assumed the algorithm already accounts for this to some extent by using the space group of the full lattice, including the non-magnetic atoms. However, a more rigorous updated approach could involve identifying all atoms along the plane of each bond and checking which symmetry operations leave the entire set of relevant atoms unchanged.

Group theory could provide more tools that could prove useful. The orbit–stabilizer theorem, which relates the number of elements in an orbit to the size of the space group and the stabilizer group of a bond by

$$|\mathrm{Orbit}| = \frac{|\mathrm{Space\ Group}|}{|\mathrm{Stabilizer}|} \tag{82}$$

In YIG, the space group has order 48. The more symmetric body diagonal bonds a have a stabilizer of order 6, meaning it appears in an orbit of length 8. The less symmetrical bonds b have stabilizer of order 2, so its orbit has length 24. This could mean that there are three times more b bonds, which matches what we find when looking at the first octant of the unit cell. This method could help identify shell anomalies when only knowing the point group of one type of bond.

Some short suggestions for further work with the algorithm are listed here. The code could be used to investigate the different symmetries of the two sublattices in $SrCu_2(BO_3)_2$ to understand arising ferrimagnetism due to unequal fluctuations of the sublattices[32]. All crystals with rutile structures should be checked for shell anomalies. More centrosymmetric materials should be investigated at the bond level for DMI allowing possible skrymions formation [18].

ACKNOWLEDGEMENTS

I'd like to thank Dr Joseph Barker for help and guidance throughout the project, and for producing the symmetry operation class facilitating the creation of the code.

[1] Ralph Skomski. *Simple models of magnetism*. Oxford graduate texts. Oxford University Press, Oxford, 2008 - 2008.

[2] Stephen Blundell. *Magnetism in Condensed Matter*. Number 4 in Oxford Master Series in Condensed Matter Physics. Oxford Univ. Press, Oxford, reprint edition, 2014.

[3] M. dos Santos Dias, N. Biniskos, F. J. dos Santos, and et al. Topological magnons driven by the Dzyaloshinskii-Moriya interaction in the centrosymmetric ferromagnet Mn_5Ge_3. *Nature Communications*, 14:7321, 2023.

[4] Lebing Chen, Jae-Ho Chung, Matthew B. Stone, Alexander I. Kolesnikov, Barry Winn, V. Ovidiu Garlea, Douglas L. Abernathy, Bin Gao, Mathias Augustin, Elton J. G. Santos, and Pengcheng Dai. Magnetic field effect on topological spin excitations in CrI_3. $Phys.Rev.X, 11 : 031047, Aug2021$.

[5] Ralph Skomski, Arti Kashyap, Jian Zhou, and David J. Sellmyer. Anisotropic exchange. *Journal of Applied Physics*, 97(10):10C713, 2005.

[6] I. E. Dzyaloshinsky. A thermodynamic theory of 'weak' ferromagnetism of antiferromagnetics. *Journal of Physics and Chemistry of Solids*, 4:241–255, 1958.

[7] Tôru Moriya. Anisotropic superexchange interaction and weak ferromagnetism. *Phys. Rev.*, 120:91–98, Oct 1960.

[8] S. W. Cheong and M. Mostovoy. Multiferroics: a magnetic twist for ferroelectricity. *Nature Materials*, 6:13–20, 2007.

[9] Frederic Keffer. Moriya interaction and the problem of the spin arrangements in $\beta\mathrm{MnS}$. *Phys. Rev.*, 126:896–900, May 1962.

[10] Andrii Chumak, Vitaliy Vasyuchka, Alexander Serga, and Burkard Hillebrands. Magnon spintronics. *Nature Physics*, 11:453–461, June 2015.

[11] A. Fert, N. Reyren, and V. Cros. Magnetic skyrmions: advances in physics and potential applications. *Nature Reviews Materials*, 2:17031, 2017.

[12] Jan Kisielewski Paweł Gruszecki. Influence of Dzyaloshinskii–Moriya interaction and perpendicular anisotropy on spin waves propagation in stripe domain patterns and spin spirals. *Scientific Reports*, 13(1):1218, 2023.

[13] A. J. Princep, R. A. Ewings, S. Ward, et al. The full magnon spectrum of yttrium iron garnet. *npj Quantum Materials*, 2:63, 2017.

[14] Mildred Dresselhaus, Gene Dresselhaus, and Ado Jorio. *Group Theory: Application to the Physics of Condensed Matter*. Springer Berlin, Heidelberg, Berlin, Heidelberg, 1 edition, 2008. Published: 18 December 2007.

[15] Gerald Burns. *Introduction to Group Theory with Applications*. Academic Press, New York, 1977.

[16] Ervin Hartmann. An Introduction to Crystal Physics. *International Union of Crystallography*, 1984.

[17] M. A. Armstrong. *Groups and Symmetry*. Undergraduate Texts in Mathematics. Springer-Verlag, New York, 1988.

[18] ShiZeng Lin. Skyrmion lattice in centrosymmetric magnets with local Dzyaloshinsky–Moriya interaction. *Materials Today Quantum*, 2:100006, 2024.

[19] Paul A. McClarty. Topological magnons: A review. *Annual Review of Condensed Matter Physics*, 13(Volume 13, 2022):171–190, 2022.

[20] M. E. Zhitomirsky and A. L. Chernyshev. Colloquium: Spontaneous magnon decays. *Reviews of Modern Physics*, 85(1):219–242, 2013.

[21] M. Malki and G. S. Uhrig. Topological magnetic excitations. *Europhysics Letters*, 132(2):20003, October 2020.

[22] Lifa Zhang, Jie Ren, Jian-Sheng Wang, and Baowen Li. Topological magnon insulator in insulating ferromagnet. *Phys. Rev. B*, 87:144101, Apr 2013.

[23] T. Holstein and H. Primakoff. Field dependence of the intrinsic domain magnetization of a ferromagnet. *Physical Review*, 58(12):1098–1113, December 1940. Received 31 July 1940; Published 15 December 1940.

[24] J Merino, Ross H McKenzie, J B Marston, and C H Chung. The heisenberg antiferromagnet on an anisotropic triangular lattice: linear spin-wave theory. *Journal of Physics: Condensed Matter*, 11(14):2965, apr 1999.

[25] F. J. Dyson. General theory of spin-wave interactions. *Physical Review*, 102(5):1217–1230, 1956.

[26] Matthias Gohlke, Alberto Corticelli, Roderich Moessner, Paul A. McClarty, and Alexander Mook. Spurious symmetry enhancement in linear spin wave theory and interaction-induced topology in magnons. *Phys. Rev. Lett.*, 131:186702, Oct 2023.

[27] Alexander Mook, Kirill Plekhanov, Jelena Klinovaja, and Daniel Loss. Interaction-stabilized topological magnon insulator in ferromagnets. *Phys. Rev. X*, 11:021061, Jun 2021.

[28] A. Corticelli, R. Moessner, and P. A. McClarty. Spin-space groups and magnon band topology. *Phys. Rev. B*, 105:064430, Feb 2022.

[29] Koichi Momma and Fujio Izumi. Vesta 3 for three-dimensional visualization of crystal, volumetric and morphology data. *Journal of Applied Crystallography*, 44:1272–1276, 2011.

[30] O. Nikotin, P.-A. Lindgärd, and O. W. Dietrich. Magnon dispersion relation and exchange interactions in MnF_2. *Journal of Physics C: Solid State Physics*, 2(7):1168–1173, 1969.

[31] Par M. Louis Néel and Louis Néel. Propriétés magnétiques des ferrites ; ferrimagnétisme et antiferromagnétisme. *Annales De Physique*, 12:137–198, 1948.

[32] Pedro M. Cônsoli, Max Fornoville, and Matthias Vojta. Fluctuation-induced ferrimagnetism in sublattice-imbalanced antiferromagnets with application to $\mathrm{SrCu_2(BO_3)_2}$ under pressure. *Phys. Rev. B*, 104:064422, Aug 2021.

[33] A. L. Chernyshev and M. E. Zhitomirsky. Spin waves in a triangular lattice antiferromagnet: Decays, spectrum renormalization, and singularities. *Phys. Rev. B*, 79:144416, Apr 2009.

[34] T. Yildirim, A. B. Harris, Amnon Aharony, and O. Entin-Wohlman. Anisotropic spin hamiltonians due to spin-orbit and coulomb exchange interactions. *Phys. Rev. B*, 52:10239–10267, Oct 1995.

[35] Libor Šmejkal, Jairo Sinova, and Tomas Jungwirth. Beyond conventional ferromagnetism and antiferromagnetism: A phase with nonrelativistic spin and crystal rotation symmetry. *Phys. Rev. X*, 12:031042, Sep 2022.

[36] Libor Šmejkal, Jairo Sinova, and Tomas Jungwirth. Emerging research landscape of altermagnetism. *Phys. Rev. X*, 12:040501, Dec 2022.

[37] Debmalya Chakraborty and Annica M. Black-Schaffer. Zero-field finite-momentum and field-induced superconductivity in altermagnets. *Phys. Rev. B*, 110:L060508, Aug 2024.

[38] S. Toth and B. Lake. SpinW: A software library for spin wave calculations. https://spinw.org, 2015.

[39] Marino M. Rybakov A. SpinW factor 2 problem. https://rad-tools.org/en/dev/_downloads/72891558945c1a7e1b83836c4f391484/magnon-dispersion.pdf.

[40] Python Core Team. *Python: A dynamic, open source programming language*. Python Software Foundation, 2023. Python version 3.12.

[41] Anubhav Jain, Shyue Ping Ong, Geoffroy Hautier, Wei Chen, William Davidson Richards, Stephen Dacek, Shreyas Cholia, Dan Gunter, David Skinner, Gerbrand Ceder, and Kristin a. Persson. The Materials Project: A materials genome approach to accelerating materials innovation. *APL Materials*, 1(1):011002, 2013.

[42] Maarten de Jong, Wei Chen, Thomas Angsten, Anubhav Jain, Randy Notestine, Anthony Gamst, Marcel Sluiter, Chaitanya Krishna Ande, Sybrand van der Zwaag, Jose J Plata, Cormac Toher, Stefano Curtarolo, Gerbrand Ceder, Kristin A. Persson, and Mark Asta. Charting the complete elastic properties of in-

organic crystalline compounds. *Scientific Data*, 2, 03 2015.

[43] Ask Hjorth Larsen, Jens Jørgen Mortensen, Jakob Blomqvist, Ivano E. Castelli, Rune Christensen, Marcin Dułak, Jesper Friis, Michael N. Groves, Bjørk Hammer, Cory Hargus, Eric D. Hermes, Paul C. Jennings, Peter Bjerre Jensen, James Kermode, John R. Kitchin, Esben Leonhard Kolsbjerg, Joseph Kubal, Kristen Kaasbjerg, Steen Lysgaard, Jón Bergmann Maronsson, Tristan Maxson, Thomas Olsen, Lars Pastewka, Andrew Peterson, Carsten Rostgaard, Jakob Schiøtz, Ole Schütt, Mikkel Strange, Kristian S. Thygesen, Tejs Vegge, Lasse Vilhelmsen, Michael Walter, Zhenhua Zeng, and Karsten W. Jacobsen. The atomic simulation environment—a python library for working with atoms. *Journal of Physics: Condensed Matter*, 29(27):273002, 2017.

[44] Atsushi Togo, Kohei Shinohara, and Isao Tanaka. Spglib: a software library for crystal symmetry search. *Science and Technology of Advanced Materials: Methods*, 4(1):2384822–2384836, 2024.

[45] Aaron Meurer, Christopher P. Smith, Mateusz Paprocki, Ondřej Čertík, Sergey B. Kirpichev, Matthew Rocklin, Amit Kumar, Sergiu Ivanov, Jason K. Moore, Sartaj Singh, Thilina Rathnayake, Sean Vig, Brian E. Granger, Richard P. Muller, Francesco Bonazzi, Harsh Gupta, Shivam Vats, Fredrik Johansson, Fabian Pedregosa, Matthew J. Curry, Andy R. Terrel, Štěpán Roučka, Ashutosh Saboo, Isuru Fernando, Sumith Kulal, Robert Cimrman, and Anthony Scopatz. Sympy: symbolic computing in python. *PeerJ Computer Science*, 3:e103, 2017.

[46] Charles R. Harris, K. Jarrod Millman, Stéfan J. van der Walt, Ralf Gommers, Pauli Virtanen, David Cournapeau, Eric Wieser, Julian Taylor, Sebastian Berg, Nathaniel J. Smith, Robert Kern, Matti Picus, Stephan Hoyer, Marten H. van Kerkwijk, Matthew Brett, Allan Haldane, Jaime Fernández del Río, Mark Wiebe, Pearu Peterson, Pierre Gérard-Marchant, Kevin Sheppard, Tyler Reddy, Warren Weckesser, Hameer Abbasi, Christoph Gohlke, and Travis E. Oliphant. Array programming with NumPy. *Nature*, 585:357–362, 2020.

[47] J. D. Hunter. Matplotlib: A 2d graphics environment. *Computing in Science & Engineering*, 9(3):90–95, 2007.

[48] Melvin Lax. *Symmetry Principles in Solid State and Molecular Physics*. Dover Publications, New York, 1974.

[49] A. A. Serga, A. V. Chumak, and B. Hillebrands. Yig magnonics. *Journal of Physics D: Applied Physics*, 43(26):264002, 2010.

[50] A. G. Gurevich and G. A. Melkov. Spin waves: Theory and applications. *Physics Reports*, 229(2):81–144, 1993.

[51] Li-Shan Xie, Guang-Xi Jin, Lixin He, Gerrit E. W. Bauer, Joseph Barker, and Ke Xia. First-principles study of exchange interactions of yttrium iron garnet. *Phys. Rev. B*, 95:014423, Jan 2017.

[52] T. Toliński and K. Synoradzki. Specific heat and magnetocaloric effect of the Mn_5Ge_3 ferromagnet. *Intermetallics*, 47:1–5, 2014.